ELSEVIER

Physica C 296 (1998) 153–166

PHYSICA C

A barrier to increasing the critical current density of bulk untextured polycrystalline superconductors in high magnetic fields

D.P. Hampshire *

Superconductivity Group, Physics Department, Durham University, Durham DH1 3LE, UK

Received 23 July 1997; accepted 6 November 1997

Abstract

The critical current density J_c in optimised untextured polycrystalline superconducting wires is still less than 1% of the depairing current density (J_d) in high magnetic fields. This paper considers whether there is a barrier to increasing J_c, of order $\ln(\kappa)/2\kappa^2$ lower than J_d (κ: Ginzburg–Landau parameter). Consideration of the wave-like properties of the superelectrons (diffraction effects) and zero pinning of fluxons that flow along normal weak-link grain boundaries leads to: $J_c(B,T) = \alpha(T)(1 - B/B_{c2}(T))\exp(-B/\beta(T))$, where for thin grain boundaries: $\alpha(T) = 0.46(H_c P^{1/2}/\lambda_{GL} S^*)(\ln(\kappa)/\kappa^2) = 0.82\, P^{1/2} B_{c2}^{3/2} \ln(\kappa)/\phi_0 \kappa^4 \mu_0 S^*$, $\beta(T) = \phi_0/2\sqrt{3}\pi d_n^{*2}$, where H_c is the thermodynamic critical field strength, S^* is the Fermi surface enhancement factor equal to one for simple metals, P is the purity parameter equal to one for clean materials, B_{c2} is the upper critical field and d_n^* is the effective thickness of the grain boundary. $\alpha(T)$ is essentially the depairing current density multiplied by a diffraction term. $\beta(T)$ characterises the suppression of the order parameter by the magnetic field at grain boundaries. The values of J_c predicted are similar to state-of-the-art wire values. © 1998 Elsevier Science B.V.

Keywords: Critical current; Flux pinning; Weak-link; Josephson effects

1. Introduction

Without doubt, the primary technological use for superconductivity has been multifilamentary wires. In such wires the critical current density (J_c) in high fields remains at less than 1% of the ultimate thermodynamic critical current density limit known as the depairing current density (J_d). Despite enormous effort, J_c in the low temperature superconducting wires NbTi and Nb_3Sn has not increased very markedly over the last 10 years. Scientists requiring very large high-field J_c in the high-temperature superconductors have found success in directing effort away from randomly aligned polycrystalline multifilamentary wires towards conductors which include very highly textured or epitaxial superconducting layers. Although our understanding of pinning and current transport has provided productive directions for increasing J_c, there is no compelling explanation for the very low J_c values relative to J_d. In this paper, we suggest that in untextured polycrystalline bulk superconductors, there is a barrier to increasing J_c of order $\ln(\kappa)/2\kappa^2$ lower than J_d.

* Tel.: +44 191 374 2167; Fax: +44 191 374 3749.

PII S0921-4534(97)01832-7

In the next section, an expression for J_d is derived and values found for $Bi_2Sr_2Ca_1Cu_2O_y$ (Bi-2212), $YBa_2Cu_3O_x$ (Y-123), $SnMo_6S_8$ (SMS), $PbMo_6S_8$ (PMS), Nb_3Sn and NbTi. In Section 3, experimental evidence is provided to demonstrate that one mechanism, related to the peak effect, determines J_c over at least part of the high magnetic field range in bulk polycrystalline untextured material. In Section 4, an expression for J_c in high fields is found by assuming that the grain boundaries are normal weak-links which act as diffracting barriers. This expression provides a framework for comparing the values of J_c for wires of different superconducting materials which is addressed in Section 5. In Section 6, the implications of this barrier for developing better wires with higher J_c are discussed.

2. The depairing current density

The depairing current density is calculated by equating the kinetic energy density of the superelectrons to the free energy density in the superconducting state [1]. In high fields this gives:

$$\frac{1}{2} m v_d^2 n_s = \frac{\mu_0 (H_{c2} - H)^2}{2.32(2\kappa^2 - 1)}, \quad (1)$$

where m is the mass of the superelectrons, v_d is the depairing velocity, n_s is the number of superelectrons per unit volume, H is the applied field strength, $\mu_0 H_{c2} = B_{c2}$ is the upper critical field and κ is the Ginzburg–Landau parameter. When the velocity of the electrons is the depairing velocity, the current density is the depairing current density (J_d) so $J_d = n e v_d$. In the high κ limit, Eq. (1) can be rewritten:

$$J_d^2 = \frac{(H_{c2} - H)^2}{2.32\kappa^2} \frac{\mu_0 n_s e^2}{m}. \quad (2)$$

More complex calculations of J_d which account for the decrease in the superconducting order parameter as the supercurrent increases typically give corrections factors of less than two and have been ignored [2]. The Hake relation [3] that gives the Ginzburg–Landau penetration depth (λ_{GL}) for dirty materials ($P \geq 1$) is:

$$\lambda_{GL}^2 = \lambda_L^2 P = \frac{m}{\mu_0 n_s e^2} \frac{1}{(S^*)^2} P, \quad (3)$$

where P is the purity parameter and $P = (\xi_0/l) \approx \lambda_{GL}^2/\lambda_L^2$, ξ_0 is the BCS coherence length, l is the electron mean free path, λ_L is the London penetration depth given by $\lambda_L^2 = m/\mu_0 n e^2$ and S^* is the Fermi surface enhancement factor where $S^* = S/S_f$ is the ratio of the free Fermi surface area S to that of a free-electron gas of the same carrier density. For clean materials, when $\xi_0/l < 1$, the London penetration depth and the Ginzburg–Landau penetration depth are the same and we take $P = 1$ when using Eq. (3). More complex calculations for λ_{GL} appropriate in the extreme clean and dirty limits which give corrections to the Hake relation of order one have been ignored [4]. In high magnetic fields, Eqs. (2) and (3) can be combined and rewritten using the Ginzburg–Landau equations $B_{c2} = \mu_0 H_{c2} = \phi_0/2\pi\xi^2$ and $\kappa = \lambda/\xi$ to give:

$$J_d = \frac{1.65 P^{1/2} B_{c2}^{3/2} (1 - b)}{\phi_0^{1/2} \kappa^2 \mu_0 S^*}, \quad (4)$$

where b ($b = B/B_{c2}$) is the reduced magnetic field. Eq. (4) can be rewritten in terms of the thermodynamic critical field strength (H_c) where $B_{c2}(T) = \sqrt{2}\,\kappa B_c$ and $B_c = \mu_0 H_c$ to give:

$$J_d = 0.93 \frac{H_c (1 - b)}{\lambda_L S^*} = 0.93 \frac{H_c P^{1/2} (1 - b)}{\lambda_{GL} S^*}. \quad (5)$$

In Table 1, values of the depairing current are listed for some of the most important technological materials. They have been calculated using fundamental parameters taken from the literature and Eq. (4) [4–13]. Literature values of either $B_{c2}(0)$ or $\xi_{GL}(0)$ are taken and the Ginzburg–Landau relation $B_{c2}(0) = \phi_0/2\pi\xi_{GL}^2(0)$ is used to derive the other parameter. In Table 1, for references cited, the subscript a denotes P calculated from $P = \lambda_{GL}^2/\lambda_L^2$, subscript b denotes P calculated from $P = \xi_0/l$. The values quoted for the purity parameter for PMS have a range from 1.5 to 7 [9]. A value of 3 has been taken for both Chevrel phase materials PMS and SMS. Similarly, since $S^* = 0.26$ for PMS, it has been assumed that the same value of S^* is reasonable for SMS. The purity and S^* parameters for the Chevrel phase materials are probably only accurate

Table 1
The fundamental parameters and depairing current density for some important technological superconducting materials

	T_c (K)	$B_{c2}(0)$ (T)	$\lambda_{GL}(0)$ (Å)	P (dimensionless)	$\epsilon_{GL}(0)$ (Å)	S/S_f (dimensionless)	$\kappa(0)$ (dimensionless)	$J_d(B=0)$ (10^{12} A m^{-2})
NbTi	9.6 [5]	14 [6]	1306 [5]	9 [5][a]	48.5	1	27	6.2
Nb_3Sn	16.1 [8]	42	930 [8]	2.96 [8][b]	28 [8]	0.4 [7]	33	31.0
$SnMo_6S_8$	14 [4]	31 [4]	2400 [9]	~ 3 [10][b]	33	0.26 [7]	73	6.2
$PbMo_6S_8$	13 [10]	56 [11]	2300 [11]	~ 3 [10][b]	24	0.26 [7]	96	8.7
$YBa_2Cu_3O_x$	92 [12]	940 [12]	1415 [12]	< 1 [13]	15	–	94	> 5.4
$Bi_2Sr_2Ca_1Cu_2O_y$	89 [12]	107 [12]	2500 [12]	< 1 [13]	18	–	139	> 1.65

The Ginzburg–Landau relations $B_{c2}(0) = \phi_0/2\pi\xi_{GL}(0)$ and $\kappa = \lambda_{GL}/\xi_{GL}$ and the Hake relation $P = (\xi_0/l) \approx \lambda_{GL}^2/\lambda_L^2$ are used to calculate a self-consistent set of fundamental parameters (discussed in the text).
The values of S^* for the high-temperature superconductors are not well known. The values of J_d have been calculated with $S^* = 1$, which gives lower bounds.
The parameters quoted for the high-temperature superconductors $YBa_2Cu_3O_x$ and $Bi_2Sr_2Ca_1Cu_2O_y$ are for B parallel to the c-axis.

to a factor 2. For clean materials, P is taken as 1 in calculating J_d. For the alloy NbTi, it has been assumed that $S^* = 1$. The values of S^* for the high-temperature superconductors are not well known — the values of J_d have been calculated with $S^* = 1$, which means they are lower bounds. The Ginzburg–Landau constant is calculated using $\kappa = \lambda_{GL}/\xi_{GL}$. Although the fundamental parameters required are not very accurately known, we expect that the values of J_d shown in Table 1 are typically accurate to a factor of ~ 3–4. It is important to note from Table 1 that J_d is two to four orders of magnitude higher than the current density achieved in bulk untextured polycrystalline superconductors.

3. High-field J_c values in the literature

In this section, J_c data for four untextured bulk superconductors in the literature are reviewed. We suggest that if the pinning is sufficiently strong, a single mechanism presents a barrier to further increases in J_c. The barrier is dependent on the fundamental superconducting properties of the material and the properties of the grain boundaries.

In Fig. 1, high-field J_c data from Friend et al. [14] for monocore Bi-2212 wire, perpendicular and parallel to the applied field are presented. Values of β are quoted in Figs. 1–4 and discussed later in Sections 4 and 5. The values of J_c in Fig. 1 are four orders of magnitude lower than the depairing current density (cf. Table 1). The exponential field dependence for J_c over much of the field range is similar to that found in the experimental and theoretical work by Hsiang and Finnemore [15] on superconducting–normal–superconducting (S–N–S) layers. This similarity suggests that current transport across the grain boundaries is critical. The data in Fig. 1 are consistent with strong intragranular pinning (in common with other high-temperature superconductors) where J_c is determined by the grain boundaries.

In Fig. 2, the bulk volume pinning force ($F_p = J_c \times B$) for three SMS samples fabricated using different thermal treatments from Bonney et al. [8] are shown. The marked contrast between the low field

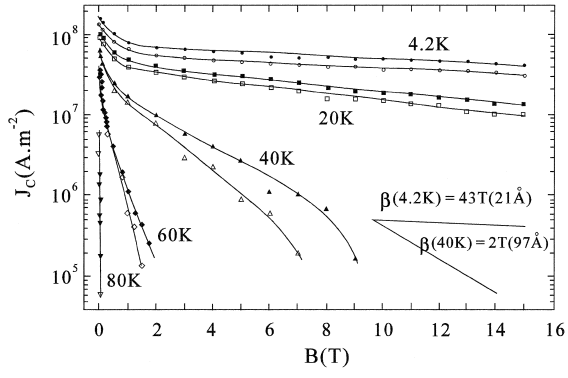

Fig. 1. $J_c(B,T)$ data for a monocore $Bi_2Sr_2Ca_1Cu_2O_y$ wire with the field parallel (closed symbols) and perpendicular (open symbols) to the wire axis [14]. Values of β are provided at 4.2 K and 40 K. The two construction lines (bottom right corner) give the approximate high field dependence for J_c and associated values of β at 4.2 K and 40 K.

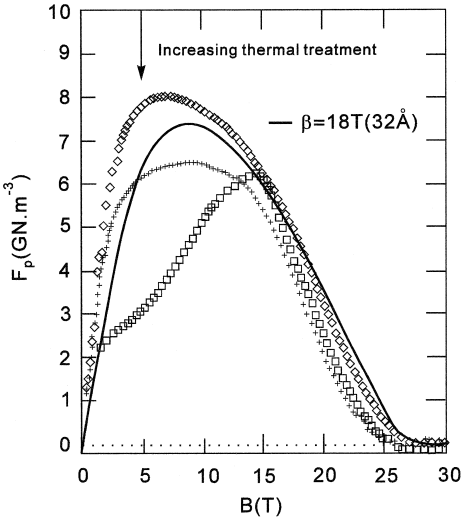

Fig. 2. The bulk volume pinning force F_p at 4.2 K for three $SnMo_6S_8$ samples fabricated using different thermal treatments. Low-field F_p is depressed with increasing thermal treatment, while at high fields F_p remains almost constant [8]. The solid curve is obtained from the weak-link diffraction model with $B_{c2} = 27$ T and $\beta = 18$ T.

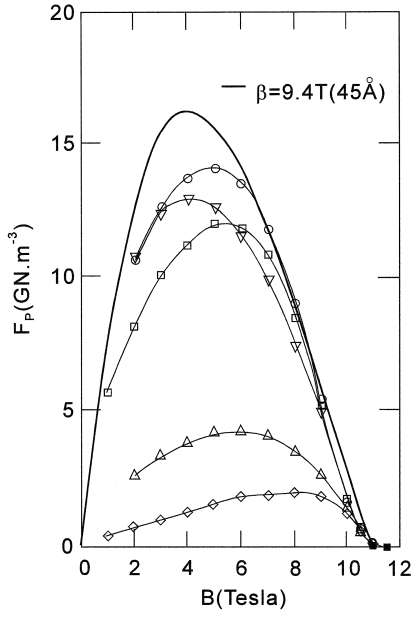

Fig. 3. The bulk volume pinning force as a function of applied field at 4.2 K for multifilamentary NbTi. Five samples with different thermomechanical treatment are shown. At low fields F_p varies by nearly an order of magnitude between the samples whereas above 10 T there is almost no difference between the samples [6]. The solid curve is obtained from the weak-link diffraction model with $B_{c2} = 11$ T and $\beta = 9.4$ T.

and high field behaviour is immediately apparent. At 5 T, F_p varies by more than a factor of two between the samples. Above 15 T, the F_p values for the different samples are almost identical. The increase in F_p for one of the samples (open-squares) is strongly suggestive of the peak-effect [16], that is a pronounced increase in F_p on approaching B_{c2}, found in many materials. The increase in F_p has been attributed to the elastic constants for the flux line lattice decreasing to zero at B_{c2} causing an improvement in the matching between the flux lines and the pinning sites [17]. However, we suggest that above 15 T, despite different grain sizes, the J_c values for these three different samples have reached a barrier to further increases.

In Fig. 3, similar characteristics occur for NbTi [6] to those of SMS in Fig. 2. Again at low fields, the values of F_p vary by a factor of 7 between the samples, presumably because of the different microstructure present. However, at high fields, notably at 10.5 T, the F_p values are almost identical.

Finally, we consider Nb_3Sn. In Fig. 4, data from Enstrom and Appert [18] replotted as volume pinning force versus reduced magnetic field at 4.2 K is

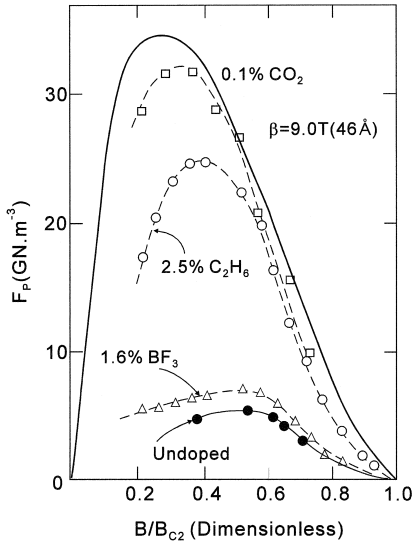

Fig. 4. The volume pinning force as a function of reduced field at 4.2 K for Nb_3Sn from Enstrom and Appert [18,19]. The labels on the curves represent concentrations of doping gases during vapour deposition of Nb_3Sn. The solid curve is obtained from the weak-link diffraction model with $B_{c2} = 20$ T and $\beta = 9$ T.

presented [19]. The Nb_3Sn material shown was fabricated with different doping gases added to the vapour during deposition. The data show similar features to those in Figs. 2 and 3. The different fabrication routes produce markedly different J_c in low fields, whereas similar values of J_c are found close to B_{c2} [19]. In Fig. 5, a compilation of F_{pmax} data is presented for bulk Nb_3Sn materials of different grain size [20–24]. F_{pmax} is defined as the maximum value of the pinning force. In bulk Nb_3Sn, F_p often obeys the Kramer dependence so that F_{pmax} occurs when $B \approx 0.2\,B_{c2} \approx 4$–5 T. The data in Fig. 5 show that the value of F_{pmax} is progressively less sensitive to grain size as the grain size decreases below about 40 nm. This result is similar to the saturation for $b > 0.7$ in the two highest pinning force Nb_3Sn materials in Fig. 4 and for SMS above 15 T in Fig. 3.

The data shown for SMS, NbTi and Nb_3Sn in Figs. 2–4 demonstrate the importance of improving the microstructure in low fields. However, we suggest that in high magnetic fields, the pinning for these materials is already sufficiently strong and the grain size sufficiently small that J_c has reached a barrier to further increases. As the grain size is reduced further, the J_c values reach this barrier over a larger range of magnetic field. For Nb_3Sn, when the grain size is sufficiently small, J_c reaches this barrier at $0.2\,B_{c2}$ and F_{pmax} becomes less sensitive to grain size. In the high T_c Bi-2212 wire, the pinning is sufficiently strong that this barrier has been reached over most of the high magnetic field range and an exponential field dependence for J_c characteristic of weak-link behaviour is found.

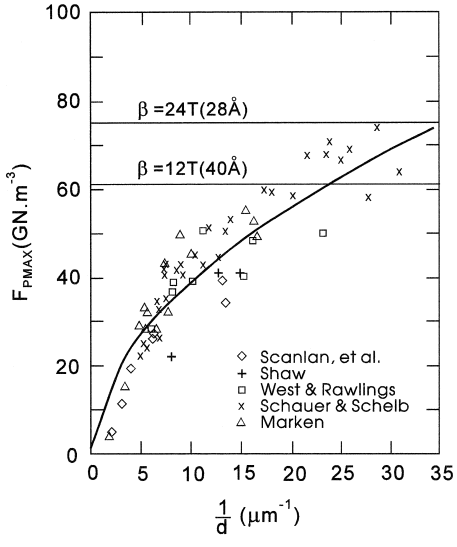

Fig. 5. Maximum pinning force per unit volume at 4.2 K as a function of reciprocal grain size in filamentary Nb_3Sn produced by bronze process. The data are from Scanlan [20], Shaw [21], West [22], Schauer and Schelb [23] and Marken [24]. The solid curve is of the form $F_{pmax} = 12.5/D^{1/2}$ (F_{pmax}: GN m^{-3}, D: μm). Values of F_{pmax} calculated using the weak-link diffraction model where $B_{c2} = 25$ T for $\beta = 16$ T and 8 T are shown.

4. High-field weak-link diffraction model

We assume that hard polycrystalline superconducting samples can be modelled by describing the grain boundaries as normal weak-links of finite thickness which act as diffracting barriers. We also assume that the intragranular pinning is sufficiently strong for the structural order in the flux line lattice to be disrupted so no pinning operates on flux moving along the grain boundaries. Under these conditions, diffraction effects caused by the wave-like properties of the superelectrons (phase-coherence) are crucial [25].

In this section, first Hsiang and Finnemore's results [15] for the critical current density through a single proximity coupled S–N–S barrier are considered. Diffraction using well-known optics and superconductivity results is then reviewed. Using the similarities between diffraction effects in optics and superconductivity, we find an expression for J_c which accounts for both the proximity effect at grain boundaries and diffraction. This provides a framework to describe the barrier to increases in J_c that has been discussed in Section 3.

4.1. Depression of the superconducting order parameter at grain boundaries

Hsiang and Finnemore [15] found an expression for the current density (ignoring diffraction effects) through a single thick clean normal barrier of the form:

$$J_c(B,T) = J_c(0)\exp\left(-\frac{B}{\beta}\right), \qquad (6)$$

where $\beta = \hbar/(2\sqrt{3}eld_n) = \phi_0/(2\sqrt{3}\pi ld_n)$, e is the charge on the electron, l is the mean free path in the normal layer and d_n is the thickness of the layer [26,27]. Eq. (6) is valid in the low field limit where

$$B \ll \frac{k_B T}{D_n e}, \tag{7}$$

where D_n is the diffusion coefficient in the normal layer. This expression can be rearranged using the relations $v_f/D_n = l_n^{-1}$ [28] (where l_n is the scattering length in the normal layer), the BCS [29] result $\xi_0 = 0.18\hbar v_f/k_B T_c$, the expression for the coherence length $\xi_{GL} = (\xi_0 l_{sc})^{1/2}$ and making the simplifying assumptions that the Fermi velocity of the electrons and the electron density are the same in the bulk and at the grain boundary. This gives

$$B \ll 0.4\left(\frac{T}{T_c}\right)\left(\frac{l_{sc}}{l_n}\right) B_{c2}(T). \tag{8}$$

Although Eq. (8) is applicable for $l_{sc} \ll l_n$, since the scaling field is B_{c2}, we use the exponential form given by Eq. (6) as a reasonable approximation throughout the field range.

Microscopic theory [30] has been used to find a value for $J_c(0)$ of the form:

$$J_c(0) = \frac{e\hbar n}{md_n}\exp\left(\frac{-d_n}{\xi_0}\right). \tag{9}$$

Eq. (9) can be rewritten:

$$J_c(0) = AJ_d(0), \tag{10}$$

where A cannot be greater than one and when less than one is given by:

$$A = \frac{3\xi_{GL}P^{1/2}}{d_n S^*}\exp\left(-\frac{d_n}{\xi_0}\right). \tag{11}$$

This confirms that if the width of the barrier is small, then the current density across the barrier in zero field is the depairing current density. Hereafter we assume that we are in the thin barrier approximation and take $A = 1$. The values for d_n found in Section 6 show this is a reasonable assumption. The field dependence of the depairing current density can be included in the expression for the current density across a single normal grain boundary so that:

$$J_c(B,T) = J_d \exp\left(-\frac{B}{\beta}\right). \tag{12}$$

4.2. Diffraction: optics and superconductivity

The similarities between the Fraunhofer diffraction pattern for light passing through a single slit and the field dependence of J_c across a weak-link are well established. In particular, the Fraunhofer pattern describing the angular distribution for the intensity of light $P(\theta)$ diffracted at an angle θ through two slits is of the form:

$$P(\theta) = P(0)\left(\frac{\sin(\beta)}{\beta}\right)^2 \cos^2(\alpha), \tag{13}$$

where $\beta = \pi b\sin(\theta)/\lambda$, $\alpha = \pi a\sin(\theta)/\lambda$, b is the width of each slit, a the separation of the slits and λ the wavelength of the light. This equation has a similar functional form to $J_c^2(B)$ for a two-junction squid given by:

$$J_c^2(B) = J_c^2(0)\left(\frac{\sin(\pi B/B_j)}{\pi B/B_j}\right)^2 \cos^2\left(\frac{\pi B}{B_l}\right), \tag{14}$$

which is known as the Josephson loop diffraction equation [31]. B is the applied field, $B_j = \phi_0/A_j$ where A_j is the area of each junction in the squid and N_0 is the fundamental flux quantum. $B_l = \phi_0/A_l$ where A_l is the area of each loop in the squid. Clearly the analogy between $P(\theta)$ and $J^2(B)$ can be extended to consider a diffraction grating with N slits or analogously a squid of N junctions in parallel so that:

$$J_c^2(B) = J_c^2(0)\left(\frac{\sin(\pi B/B_j)}{\pi B/B_j}\right)^2 \times \left(\frac{\sin(N\pi B/B_l)}{N\pi B/B_l}\right)^2. \tag{15}$$

In Fig. 6, the intensity diffraction pattern for a multiple slit grating is shown (lower and left-hand axes). It is assumed that there are N slits in the grating and each of the slits is very narrow ($b \ll \lambda$) and separated by a distance a. In the figure, N has

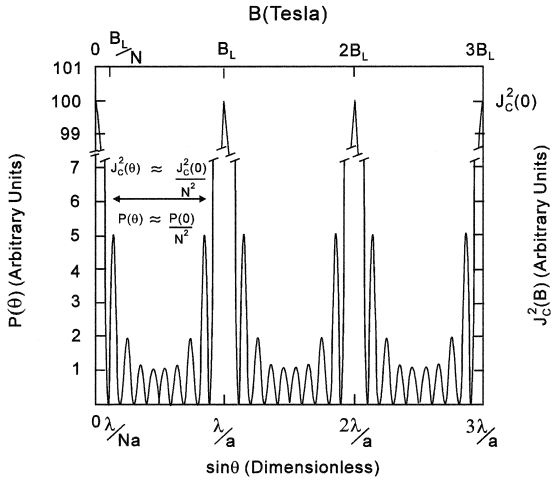

Fig. 6. The diffraction pattern for N-slits separated by a, illuminated by light of wavelength λ. $P(\theta)$ is the angular intensity diffracted at an angle θ (bottom and left-hand axes). It is assumed that $N = 10$ and the width of the slits is very small relative to λ. The figure also represents the current density squared $J_c^2(B)$ as a function of field for an N-junction squid where $B_1 = \phi_0 / A_1$ and A_1 is the area of each loop in the squid (top and right-hand axes). It is assumed that the area of each junction in the squid is very small.

arbitrarily been set to be 10. The diffraction pattern has major peaks of intensity $P(0)$ between which the intensity is approximately $P(0)/N^2$. This result follows from Eq. (13) since for $\alpha \to 0,\ \pi,\ 2\pi, \ldots,$ $(\sin(N\alpha)/\sin(\alpha))^2 \to N^2$, whereas in general $\sin^2(N\alpha) \approx 1$ and $\sin^2(\alpha) \approx 1$, so $((\sin(N\alpha)/\sin(\alpha))^2 \approx 1$.

We note two additional properties for diffraction gratings. First, the diffraction pattern can be truncated. Since $\sin(\theta) \leq 1$, by setting a equal to λ there is no physical significance to values of $\sin(\theta)$ greater than λ/a. Second, if a series of sequential gratings are replaced by an equivalent single grating, the single grating slit size must be much smaller than the size of slits in the components of the sequential diffraction gratings. This follows since the light diffracted through the first grating is diffracted again as it passes through the second grating. The effect of a large number of many such gratings will be to cause large amounts of light to be scattered to large angles. Hence, as the number of gratings in the sequential diffraction increases, the slit size of the equivalent single grating decreases.

4.3. Diffraction at grain-boundaries

In granular high-temperature superconductors, the precipitous drop of J_c in very low fields (< 5 mT) has been attributed to the weak-link (diffraction) properties of the grain boundaries [25]. Indeed diffraction limited J_c values have been produced in single grain boundary junctions using high-temperature superconductors [32]. However, the exponential dependence derived in Section 4.1 which accounts for the proximity effect at the normal weak-link ignores diffraction effects. In this section, we find an expression which includes diffraction.

First, essentially a dimensionality argument is used. It is assumed that a multiple junction squid of appropriate geometry can be used to describe the diffraction effects that determine the current density through a polycrystalline superconductor. Physical arguments are used to find the geometry of the squid which provides an estimate for the field dependence of $J_c(B)$. The diffraction pattern in Fig. 6 describes the current density squared through an N-junction squid (upper and right-hand axes) where the area of each junction is small ($A_j \ll \phi_0/B$). In order to ensure that there are no major peaks between the lower critical field (B_{c1}) and the upper critical field (B_{c2}), B_1 is set equal to B_{c2}. This result implies $A_1 \approx 2\pi\xi^2$. This small loop area is consistent with sequential scattering through many grain boundaries being equivalent to diffraction through a single N-junction squid with loop areas much smaller than the grain boundary size. Below B_{c1}, if the self-field of the critical current is ignored, the intragranular pinning is assumed to be very strong and the grain boundaries very thin, there are no fluxons in the sample and the current density is equal to the depairing current density ($J_c(0)$). This leads to setting $B_1/N = B_{c1}$. Hence for an N-junction squid where the area of each loop in the squid is $2\pi\xi^2$ and N is B_{c2}/B_{c1}, between B_{c1} and B_{c2}, Fig. 6 shows that $J_c(B)$ can be approximated by:

$$J_c(B) = \frac{J_c(0)}{N} = J_c(0)\frac{B_{c1}}{B_{c2}}. \qquad (16)$$

Using the Ginzburg–Landau relations $B_{c1} = B_c \ln(\kappa)/\sqrt{2}\kappa$ and $B_{c2} = \sqrt{2}\kappa B_c$ this gives:

$$J_c(B) = J_d \frac{\ln(\kappa)}{2\kappa^2}. \qquad (17)$$

We have assumed (without proof) that the diffraction properties of a polycrystalline material can be effectively described by a multiple junction squid. The geometry of the squid has been proscribed by assuming the current density first drops at B_{c1}, there are no primary peaks in J_c between B_{c1} and B_{c2}, and J_c drops to zero above B_{c2}. Although the geometry is not uniquely specified, Eqs. (16) and (17) result.

A more rigorous justification for Eqs. (16) and (17) is as follows. Consider light passing through a single circular aperture. The light diffracts forming a primary solid cone of light. The intensity of light within the angle of slant for the cone (θ_{min}) can be defined as $P(0)$. If a large number of additional apertures, which are randomly oriented, are then inserted so that all the light sequentially diffracts many times, eventually the light will travel in all directions with uniform intensity ($P(\theta)$). The independence of $P(\theta)$ to angle is a general result that follows from multiple sequential diffraction and not on the size of the additional apertures inserted. The maximum angle of diffraction (θ_{max}) is simply π radians for this optical case. The ratio of the intensities $P(\theta)/P(0)$ is the ratio of the solid angles in the two cases, so $P(\theta)/P(0) = (\theta_{min})^2/(\theta_{max})^2$. We now apply this result to bulk polycrystalline superconductors. Consider subdividing a bulk superconductor into a series of filaments of diameter approximately equal to the Ginzburg–Landau penetration depth. The size of the filaments facilitates using diffraction equations and ensures that below B_{c1}, no flux penetrates the material. We use the result for the ratio of the intensities ($P(\theta)/P(0)$) found for the optical analogue to give the effect of the grain boundaries acting as sequential diffracting barriers in the filament. Equating $P(\theta)$ to $J_c^2(B)$, $P(0)$ to $J_c^2(0)$, θ_{min} to B_{c1} and θ_{max} to B_{c2} we again find the results given by Eqs. (16) and (17). Hence we find a simple physical explanation for the field independent term $\ln(\kappa)/2\kappa^2$ in Eqs. (16) and (17). In a single barrier one can consider the phase to be constant in a direction orthogonal to the current flow. Inserting fluxons into the barrier profoundly affects the interference conditions and hence the current that can flow across the barrier. However, after multiple diffraction through many barriers, the phase is considerably randomised and this constant phase approximation is no longer valid. In this case fluxons in the barrier have no effect on the interference conditions and the effect of the multiple diffraction is a field independent term. In summary, if the intragranular pinning is strong and there is no pinning operating for flux motion along the grain boundaries, the grain boundaries can be considered as diffraction barriers. Between B_{c1} and B_{c2}, the current density is independent of grain size and reduced from $J_c(0)$ by $\ln(\kappa)/2\kappa^2$.

4.4. The functional form of $J_c(B,T)$

We combine Eqs. (12) and (17) to give an expression for the critical current density in high fields. It accounts for the reduction in the depairing current density caused by depression of the order parameter by the magnetic field at the grain boundaries and diffraction effects, which is of the form:

$$J_c(B,T) = \alpha(T)\left(1 - \frac{B}{B_{c2}(T)}\right)\exp\left(-\frac{B}{\beta(T)}\right), \tag{18}$$

where for thin grain boundaries:

$$\alpha(T) = 0.46\left(\frac{H_c\, P^{1/2}}{\lambda_{GL}\, S^*}\right)\left(\frac{\ln(\kappa)}{\kappa^2}\right) = \frac{0.82\, P^{1/2}\, B_{c2}^{3/2}\ln(\kappa)}{\phi_0\,\kappa^4\mu_0 S^*},$$

$$\beta(T) = \frac{\phi_0}{2\sqrt{3}\,\pi\, l d_n}.$$

Rearranging the expression for β and setting the effective weak-link thickness d_n^* equal to $(d_n l)^{1/2}$ gives:

$$d_n^* = \frac{138}{\beta^{1/2}}, \tag{19}$$

where d_n^* is in Angstroms and β is in Tesla. In all the figures in this work where values of β are provided in Tesla, equivalent values in Å are also given.

5. Predictions of high field weak-link diffraction model

First the field dependence of Eq. (18) is considered, in particular the factors $(1 - B/B_{c2}(T))$ and $\exp(-B/\beta)$. In Fig. 7, J_c versus field for different

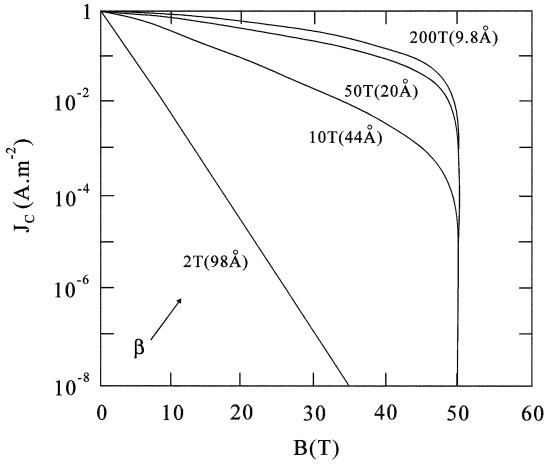

Fig. 7. The calculated current density (J_c) for a randomly oriented bulk polycrystalline superconductor as a function of β. J_c is calculated using the weak-link diffraction model, where $J_c(B=0)$ is set equal to 1 and B_{c2} is set equal to 50 T.

values of β is presented. J_c has arbitrarily been set equal to 1 A m^{-2} at $B=0$ and B_{c2} set equal to 50 T. In Fig. 8, the equivalent F_p values have been plotted as a function of field. For values of β much larger than B_{c2}, the change in J_c due to the exponential factor is small so J_c is approximately proportional to $(1-B/B_{c2}(T))$ and F_p has a peak value at about $0.5B_{c2}$ (cf. Fig. 8, $\beta=200$ T). As β decreases, the peak value in F_p moves to lower values of field. Eventually, when β is much smaller than B_{c2}, the exponential field dependence dominates (cf. Fig. 7, $\beta=2$ T). It is interesting to note that for $\beta=10$ T, F_p has a peak value at $B.\ 0.2B_{c2}$. This is the same as that found for the Kramer dependence [19] which occurs in many superconductors. Even for $\beta=2$ T, on a volume pinning force plot of the type shown in Fig. 8, the peak in the volume pinning force also occurs for $B\approx 0.2B_{irr}$, if B_{irr} is defined as the field at which F_p linearly extrapolates to zero [33].

Comparing experimental values of J_c with the functional form given by Eq. (18), the free parameter that determines the field dependence is β. The data for Bi-2122 in Fig. 1 are exponential over a large field range with values of β of 43 T (21 Å) at 4.2 K and 2 T (97 Å) at 40 K. Extrapolating J_c to $B=0$ at 4.2 K gives a value less than 10^8 A m^{-2} compared to a lower bound calculated value from Eq. (11) of about 2×10^8 A m^{-2}. This discrepancy is certainly within the uncertainty given for the fundamental constants for the material. We note that 19 filament Bi-2212, which is less susceptible to cracks gives an extrapolated value for $J_c(0)$ closer to the calculated value. In Fig. 2, the solid curve for SMS is generated using Eq. (11) where B_{c2} was set at 27 T and β at 18 T (32 Å). All other fundamental parameters for SMS were taken from Table 1. The calculated values of J_c are in good agreement above 15 T, but are about a factor of 2 smaller at low fields. In Fig. 3, the solid curve for NbTi has been calculated using $B_{c2}=11$ T and $\beta=9.4$ T (45 Å). In Fig. 4, the solid curve shown has been calculated using $B_{c2}=20$ T and $\beta=9.0$ T (46 Å). The values of F_{pmax} in Fig. 5 for Nb_3Sn have been calculated for $\beta=12$ T (40 Å) and 24 T (28 Å) using $B_{c2}=25$ T. Fig. 5 shows how the values for F_{pmax} can increase if the effective width of the grain boundaries decreases. Comparing the solid curves in Figs. 2–4 with the experimental data, the agreement at high fields is better than that at low fields. In the context of depairing current densities that are two-to-four orders of magnitude higher than J_c in the wires, given the uncertainties in the fundamental parameters, we suggest that there is rather good agreement between the experimental data and the calculated values of high field current den-

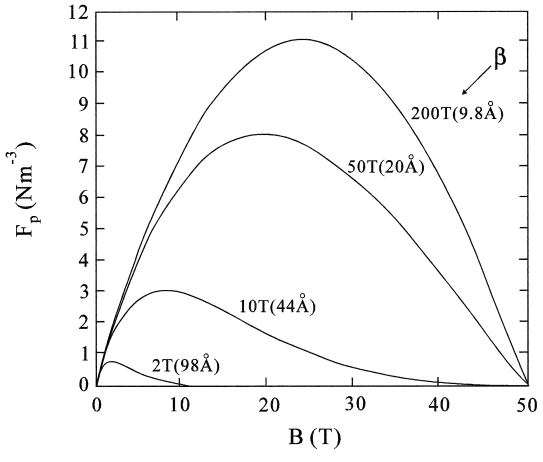

Fig. 8. The calculated volume pinning force (F_p) for a randomly oriented bulk polycrystalline superconductor as a function of β. F_p is calculated using the weak-link diffraction model, where $F_p=J_c\times B$, $J_c(B=0)$ is set equal to 1 and B_{c2} is set equal to 50 T.

sity given by Eq. (18) that includes a two-parameter fit for β and B_{c2}.

6. Discussion

The conventional explanation for the low J_c values in low temperature superconductors has been that the pinning is not sufficiently strong. However, it is difficult to explain the peak effect that is found in many materials (e.g. the saturation in Figs. 2–4) exclusively in those terms. One might expect that as the pinning density increased, J_c increased broadly monotonically. In this paper a different interpretation for optimising J_c in bulk polycrystalline superconductors is proposed. Optimising J_c is a process of increasing the intragranular pinning and improving the properties of the grain boundaries. Eventually when the intragranular pinning is sufficiently strong, the critical current density is limited by the current that can be transmitted across the grain boundaries.

We have suggested: there is experimental evidence for a barrier to increases in J_c in bulk untextured polycrystalline superconductors, of order $\ln\kappa/2\kappa^2$ below J_d; the functional form for J_c at this barrier is determined by the fundamental superconducting properties of the superconductor and the grain boundaries of the material; this functional form can be found using a weak-link diffraction model. These suggestions are discussed in this section.

6.1. Experimental evidence for a barrier well below J_d

Kramer [34,35] concluded that the peak effect was characteristic of a flux shear mechanism where free fluxons, in a perfectly hexagonal lattice, plastically shear past pinned fluxons. His work provided an explanation for the weak microstructural dependence of J_c in high fields. However, since the original work, the elastic constants (C_{66}) have been recalculated [36]. Inserting the correct functional form for C_{66} changes the functional form from that originally predicted by Kramer's model and used to fit the data [37]. Nevertheless, Kramer [34,35] reviewed experimental data for a broad range of superconducting materials which show the peak effect including the intermetallic superconductors Nb_3Sn, V_3Ga, NbN and Nb_3Al and ductile alloys such as NbTi, NbTa and NbMo. He concluded that close to B_{c2}, J_c is broadly independent of microstructure. Figs. 2–4 show J_c values which are insensitive to microstructure in high magnetic fields that we suggest have reached a barrier to further increases.

In Table 2 the magnitude of J_c is considered. The values of T_c and J_d are included from Table 1. The factor $\ln\kappa/2\kappa^2$ is calculated and multiplied by J_d to give the critical current density (J_{calc}) (cf. Eqs. (17) and (18)) at $B = 0$. Also shown are values of critical current density (J_{litt}(Peak)) from the literature (cf. Figs. 1–4) at 4.2 K at the field given by $F_p = F_{pmax}$. By taking J_{litt}(Peak) defined in this way, the values are characteristic of high field values and can be compared to J_{calc}.

In Fig. 9, J_{litt}(Peak) versus J_{calc} are plotted for the different superconducting materials considered in this work. The solid line on the figure defines J_{litt}(Peak) equals J_{calc}. The shaded region gives typical values of depairing currents. We suggest that the Bi-2212 film [38] in Fig. 9 is well above the solid line because the material is strongly textured so that

Table 2
A comparison between the critical current density at $B = 0$ predicted using the weak-link diffraction model J_{calc} and state-of-the-art values J_{litt}(peak) found in the literature at the peak in the pinning force

	T_c (K)	J_d (10^{12} A m^{-2})	ln $\kappa/2\kappa^2$ (10^{-3})	J_{calc} (10^9 A m^{-2})	J_{litt}(Peak) (10^9 A m^{-2})
Nb-38 at% Ti	9.6	6.2	2.26	14	5 [6]
Nb_3Sn	16.1	31.0	1.6	50	15 [4]
$SnMo_6S_8$	14	6.2	0.40	2.5	1.2 [8]
$PbMo_6S_8$	13	8.7	0.25	2.2	4 [41]
$YBa_2Cu_3O_x$	92	>5.4	0.257	>1.4	0.001 [45]
$Bi_2Sr_2Ca_1Cu_2O_y$	89	>1.65	0.127	>0.21	0.15 [14]

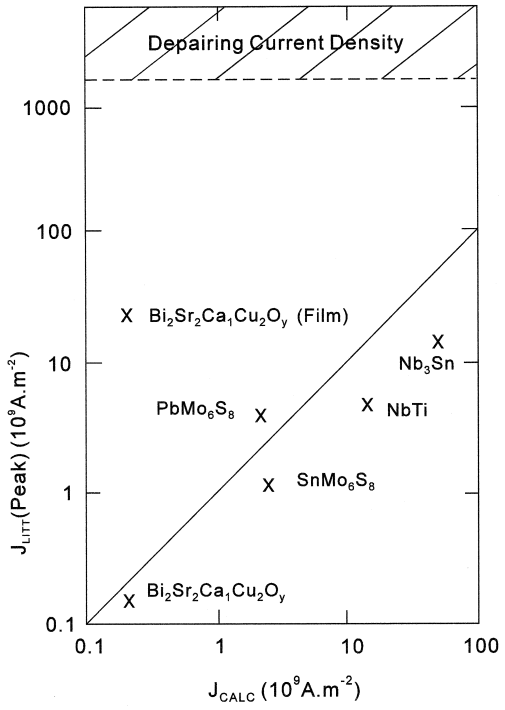

Fig. 9. A comparison between the current density found in optimised bulk superconducting materials and those calculated using the weak-link diffraction model. J_{litt}(Peak) is the value of the current found experimentally at the maximum pinning force. J_{calc} is the calculated value of current density in zero field using the weak-link diffraction model. The shaded region shows typical values of the depairing current for the materials shown.

grain boundaries do not act as barriers to current flow. In addition, surface currents may play a role in these materials [39]. The highest reported J_c values in Bi-2223 are also found in epitaxial thin films that are apparently devoid of grain boundaries [40]. The PMS probably lies above the line because of uncertainties in the fundamental parameters for this material although some degree of texturing cannot be ruled out [41]. We suggest that Nb_3Sn, NbTi, SMS and Bi-2212 which lie below the solid line are characteristic of bulk untextured polycrystalline superconductors with strong pinning and grain boundaries approximately 2–4 nm thick. The $YBa_2Cu_3O_x$ (not shown) has a very low J_c either because the grain boundaries have a large effective thickness or the intragranular pining is not very strong [42].

6.2. The weak-link diffraction model

The short coherence length of the high-temperature superconductors is consistent with strong intragranular pinning and weak-link grain boundaries. By using the weak-link diffraction model universally, we are implicitly implying a similar description for the low temperature superconductors and the Chevrel phase superconductors. In superconductors optimised for high J_c, the inhomogeneities (e.g. disruption of the Nb chains in Nb_3Sn [43], sulphur defects in SMS [44]) will certainly produce pinning. Whether these effects can lead to sufficiently strong intragranular pinning that the intergranular current becomes the limiting factor is not proven. In the context of conventional pinning theory, reducing the grain size increases the grain boundary area per unit volume and hence the density of pinning sites [45]. The weak-link diffraction model suggests that reducing the grain size may be effective because it leads to stronger intragranular pinning. The model may also help explain the very weak dependence of J_c to the orientation of the applied field as shown for Bi-2212 in Fig. 1 and also found in NbTi [46].

The values for β found experimentally and related through Eq. (18) to an effective thickness give values of 2–4 nm which are not physically unreasonable. Strain measurements on the Nb_3Sn and PMS show that a strain as small as 0.3% can reduce B_{c2} by 10% [47]. The grain boundary strain field, structure and disorder may be the origin of the weak-link behaviour and determine the effective grain boundary thickness. High field measurements on high-temperature superconductors [26], and Chevrel phase superconductors $PbMo_6S_8$ and $(Pb_{1-x}Gd_x)Mo_6S_8$ [48] show that β decreases as the temperature increases. This is consistent with the effective thickness of the weak-link grain-boundaries increasing as the temperature approaches T_c [49].

The Hsiang and Finnemore proximity expression was derived for thick normal barriers in the clean limit. It has been pointed out that this may not be appropriate for grain boundaries [15]. Further calculations are required to determine d_n^* and the effect of strong intragranular pinning on the fluxon–fluxon interactions of fluxons within a grain boundary. Such work will determine whether there is pinning of flux

as it moves along grain boundaries. It is clearly important in the texturing of superconductors whether the grain boundaries (indeed any extended defects such as twin boundaries) act as pinning free diffraction barriers or regions of strong pinning. One can relatively easily distinguish the extreme cases experimentally by measuring the field dependence of J_c to find either a diffraction pattern or a pinning mechanism. However, to understand the properties of grain boundaries in general, detailed investigation of the structure and electronic properties at grain boundaries on the scale of the coherence length will be required to correlate microprobe and electron microscopy measurements with experimental values of β determined from high field J_c data.

An interesting feature of the functional form of Eq. (18) is the relationship between β and the reduced field at which the peak in the pinning force (F_{pmax}) occurs. The different field dependencies for J_c found for the materials in Figs. 1–4 are usually attributed to different pinning mechanisms operating. This can occur because the microstructure and the atomic bonding found in the alloy NbTi, the Chevrel phase SMS, the intermetallic Nb_3Sn and the high-temperature superconductor Bi-2212 (which can be classified as a ceramic) differ markedly. However, we have found that in NbTi where $\beta \approx B_{c2}$, F_{pmax} occurs at about $0.5B_{c2}$. For Nb_3Sn and SMS where β is lower than B_{c2}, F_{pmax} occurs at about $0.2\,B_{c2}$. For Bi-2212, where β is very small compared to $B_{c2}(T)$, J_c is exponential. These results are consistent with Eq. (18) and Figs. 7 and 8 and in the context of the weak-link diffraction model suggest that the field dependence of J_c in these materials is determined by the relative magnitude of B_{c2} and the effective thickness of the grain boundaries. We also note with interest that if $d_n^* \propto \xi_{GL}(T)$ then Eq. (18) has the form required to produce a universal flux pinning scaling law [50].

The weak-link diffraction model is a considerable departure from pinning models used to describe hard type II superconductors in high fields which do not consider phase coherence. Future work will include an analysis of three-dimensional current flow in polycrystalline samples. Detailed numerical calculations which include the diffracting properties of grain boundaries and percolative current flow in polycrystalline samples are required to determine whether the physical arguments used in Section 4 accurately describe the properties of the weak-link diffraction model proposed. If phase coherence is critical in determining J_c in optimised polycrystalline superconductors, it is probably critical in achieving the optimisation. The data in Fig. 5 were originally used to provide evidence for a $F_{pmax} \propto 1/D$ (D: grain size) dependence characteristic of pinning. The solid line we have added is of the form $F_{pmax} = 12.5/D^{1/2}$ (F_{pmax}: GN m^{-3}, D: μm) which can equally well describe the data. However, calculating the role of phase coherence in optimising J_c in polycrystalline materials is beyond the scope of this work.

6.3. Future work on improving J_c

Historically, reducing grain size (cf. Fig. 5) has improved J_c in low temperature superconductors. However, in high-temperature superconductors effort is directed at improving the texturing of materials leading to larger grain size. It is suggested in this work that there is a barrier to increasing J_c in bulk polycrystalline superconductors which can explain the efficacy of these two apparently contradictory approaches.

This work implies that further significant increases in J_c in high fields will only be achieved in superconductors by including strong pinning in highly textured or single-crystalline material. Melt-texturing and IBAD offer obvious choices [51] which should be effective for low temperature and high-temperature superconductors. Small grain boundaries can facilitate strong pinning but inevitably introduce a barrier which limits the maximum value of high-field J_c to far below the depairing current.

We suggest that high field critical current data could usefully be parametrised in the form:

$$J_c(B,T) = \alpha(T)\left(1 - \frac{B}{B_{c2}(T)}\right)\exp\left(-\frac{B}{\beta(T)}\right), \tag{20}$$

where $\alpha(T)$, $\beta(T)$ and $B_{c2}(T)$ are all free parameters. If the intragranular pinning is strong throughout the field range, $B_{c2}(T)$ will give the upper critical field of the grains, $\beta(T)$ can be directly related to the effective thickness of the grain boundaries and $\alpha(T)$ can be compared to values given by Eq. (18) as a measure of whether the material is optimised.

7. Conclusions

In this paper it has been suggested that:

(i) In bulk polycrystalline superconductors, if the intragranular pinning is very strong, there is a barrier to increases in J_c that is a factor $\ln(\kappa)/2\kappa^2$ below the depairing current.

(ii) The functional form for J_c at this barrier is given by:

$$J_c(B,T) = \alpha(T)\left(1 - \frac{B}{B_{c2}(T)}\right)\exp\left(-\frac{B}{\beta(T)}\right), \tag{21}$$

where for thin grain boundaries:

$$\alpha(T) = 0.46\left(\frac{H_c P^{1/2}}{\lambda_{GL} S^*}\right)\left(\frac{\ln(\kappa)}{\kappa^2}\right) = \frac{0.82\, P^{1/2} B_{c2}^{3/2}\ln(\kappa)}{\phi_0 \kappa^4 \mu_0 S^*},$$

$$\beta(T) = \frac{\phi_0}{2\sqrt{3}\,\pi l d_n} = \frac{\phi_0}{2\sqrt{3}\,\pi d_n^{*2}}.$$

(iii) Physical arguments have been used to support a weak-link diffraction model which has been proposed to determine the critical current density (J_c). It is assumed that there is strong intragranular pinning and the grain boundaries are normal weak-links which act as diffraction barriers.

(iv) Rather good agreement is found between the weak-link diffraction model and high field experimental data. The model leads to values for grain boundary thicknesses of 2–4 nm which can be explicitly tested in future work.

Acknowledgements

The author thanks members of the Superconductivity Group for useful discussions.

References

[1] M. Tinkham, Introduction to Superconductivity, McGraw-Hill, New York, 1996.
[2] J. Bardeen, Rev. Mod. Phys. 34 (1962) 667.
[3] R.R. Hake, Phys. Rev. 158 (1966) 356.
[4] T.P. Orlando, E.J. McNiff, S. Foner, M.R. Beasley, Phys. Rev. B 19 (1979) 4545.
[5] E.W. Collings, in: K.D. Timmerhaus, A.F. Clark (Eds.), Applied Superconductivity, Metallurgy and Physics of Titanium Alloys, Plenum Press, New York, 1986, pp. 490–491.
[6] J.V.A. Somerkoski, D.P. Hampshire, H. Jones, R.O. Toivanen, V.K. Lindroos, IEEE Trans. Magn. 23 (1987) 1629.
[7] J.A. Woolam, S.A. Alterovitz, Phys. Rev. B 19 (1979) 749.
[8] L.A. Bonney, T.C. Willis, D.C. Larbalestier, J. Appl. Phys. 77 (1995) 6377.
[9] P. Birrer, F.N. Gygax, B. Hitti, E. Lippelt, A. Schenck, M. Weber, D. Cattani, J. Cors, M. Decroux, O. Fischer, Phys. Rev. B 48 (1993) 16589.
[10] C. Rossel, Thesis No. 2019, University of Geneva, 1981.
[11] D.N. Zheng, H.D. Ramsbottom, D.P. Hampshire, Phys. Rev. B 52 (1995) 12931.
[12] D.R. Harshman, A.P. Mills Jr., Phys. Rev. B 45 (1992) 10684.
[13] G. Deutscher, Physica C 153–155 (1988) 15.
[14] C.M. Friend, J. Tenbrink, D.P. Hampshire, Physica C 258 (1995) 213.
[15] T.Y. Hsiang, D.K. Finnemore, Phys. Rev. B 22 (1980) 154.
[16] D.M. Kroeger, Solid State Commun. 7 (1969) 843.
[17] A.B. Pippard, Phil. Mag. 19 (1969) 220.
[18] R.E. Enstrom, J.R. Appert, J. Appl. Phys. 43 (1973) 1915.
[19] E.J. Kramer, J. Appl. Phys. 44 (1973) 1360.
[20] R.M. Scanlan, W.A. Fietz, E.F. Koch, J. Appl. Phys. 46 (1975) 2244.
[21] B.J. Shaw, J. Appl. Phys. 47 (1977) 2143.
[22] A.W. West, R.D. Rawlings, J. Mater. Sci. 12 (1977) 1862.
[23] W. Schauer, W. Schelb, IEEE Trans. Magn. 17 (1981) 374.
[24] K. Marken, Ph.D Thesis, University of Wisconsin, 1986.
[25] R.L. Peterson, J.W. Ekin, Phys. Rev. B 42 (1990) 8014.
[26] L. LeLay, C.M. Friend, T. Maruyama, K. Osamura, D.P. Hampshire, J. Phys. C 6 (1994) 10053.
[27] D.P. Hampshire, S.-W. Chan, J. Appl. Phys. 72 (1992) 4220.
[28] A.B. Pippard, The Dynamics of Conduction Electrons, Gordon and Breach, New York, 1965, p. 35.
[29] J. Bardeen, L.N. Cooper, J. Schrieffer, Phys. Rev. 108 (1957) 1175.
[30] V.P. Galaiko, A.V. Svidzinskii, V.A. Slyusarev, JETP 29 (1969) 454.
[31] E. Hecht, A. Zajac, Optics, Addison-Wesley, 1974.
[32] C.P. Poole, Jr., H.A. Farach, R.J. Creswick, Superconductivity, Academic Press, New York, 1995.
[33] D.P. Hampshire, EUCAS 93, DGM Informationsgesellschaft, Oberusel, 1993, p. 873.
[34] E.J. Kramer, J. Electron. Mater. 4 (1975) 839.
[35] K.E. Osbourne, E.J. Kramer, Phil. Mag. 29 (1974) 685.
[36] E. Brandt, Phys. Status Solidi B 77 (1976) 551.
[37] D.P. Hampshire, H. Jones, E.W.J. Mitchell, IEEE Trans. Magn. 21 (1984) 289.
[38] P. Schmitt, P. Kummeth, L. Schultz, G. Saemann-Ischenko, Phys. Rev. Lett. 67 (1991) 267.
[39] G. Stejic, A. Gurevich, E. Kadyrov, D. Christen, R. Joynt, D.C. Larbalestier, Phys. Rev. B 49 (1994) 1274.

[40] H. Yamasaki, K. Endo, S. Kosaka, M. Umeda, S. Yoshida, K. Kajimura, Phys. Rev. Lett. 70 (1993) 3331.
[41] N. Cheggour, M. Decroux, A. Gupta, O. Fischer, J.A.A.J. Perenboom, V. Bouquet, M. Sergent, R. Chevrel, J. Appl. Phys. 81 (1977) 6277.
[42] K. Heine, J. Tenbrink, M. Thoner, Appl. Phys. Lett. 55 (1989) 2441.
[43] A.R. Swedler, D.G. Schweitzer, G.W. Webb, Phys. Rev. Lett. 33 (1974) 168.
[44] H. Yamasaki, Y. Yamaguchi, Y. Kimura, Mater. Res. Bull. 23 (1988) 23.
[45] D. Dew-Hughes, Phil. Mag. 30 (1974) 293.
[46] C.M. Friend, D.P. Hampshire, EUCAS 93, DGM Informationsgesellschaft, Oberusel, 1993, p. 23.
[47] J.W. Ekin, T. Yamashita, K. Hamasaki, IEEE Trans. Magn. 21 (1985) 474.
[48] D.N. Zheng, S. Ali, H.A. Hamid, C. Eastell, M. Goringe, D.P. Hampshire, Physica C 291 (1997) 49.
[49] K. Osamura, S. Nonaka, M. Matsui, T. Oku, S. Ochiai, D.P. Hampshire, J. Appl. Phys. 79 (1996) 7877.
[50] R.G. Hampshire, M.T. Taylor, J. Phys. F 2 (1972) 89.
[51] P. Grant, Nature 375 (1995) 107.